






## RESEARCH ARTICLE

# Roles of *Cep215/Cdk5rap2* in establishing testicular architecture for mouse male germ cell development

Donghee Kang<sup>1</sup>  | Byungho Shin<sup>1</sup>  | Gyeong-Nam Kim<sup>2,3</sup> | Ji Hwa Hea<sup>2,3</sup>  |  
Young Hoon Sung<sup>2,3</sup>  | Kunsoo Rhee<sup>1</sup> <sup>1</sup>Department of Biological Sciences, Seoul National University, Seoul, Korea<sup>2</sup>Department of Cell and Genetic Engineering, Asan Medical Center, University of Ulsan College of Medicine, Seoul, Korea<sup>3</sup>Asan Institute for Life Sciences, Convergence mEDicine research cenTer (CREDIT), Asan Medical Center, Seoul, Korea**Correspondence**

Kunsoo Rhee, Department of Biological Sciences, Seoul National University, Seoul 08826, Korea.

Email: [rhee@snu.ac.kr](mailto:rhee@snu.ac.kr)

Young Hoon Sung, Department of Cell and Genetic Engineering, University of Ulsan College of Medicine, Seoul 05505, Korea.

Email: [yhsung@amc.seoul.kr](mailto:yhsung@amc.seoul.kr)**Funding information**

National Research Foundation of Korea (NRF), Grant/Award Number: RS-2024-00344272 and 2014M3A9D5A01075128; Korea Health Industry Development Institute (KHIDI), Grant/Award Number: HI21C169202; Asan Institute for Life Sciences, Asan Medical Center, Grant/Award Number: 2021IP0050

**Abstract**

*Cep215/Cdk5rap2* is a centrosome protein crucial for directing microtubule organization during cell division and morphology. *Cep215* is a causal gene of autosomal recessive primary microcephaly type 3, characterized by a small brain size and a thin cerebral cortex. Despite previous attempts with *Cep215* knockout (KO) mice to elucidate its developmental roles, interpreting their phenotypes remained challenging due to potential interference from alternative variants. Here, we generated KO mice completely lacking the *Cep215* gene and investigated its specific contributions to male germ cell development. In the absence of *Cep215*, testis size decreased significantly, accompanied by a reduction in male germ cell numbers. Histological analyses unveiled the arrested development of male germ cells around the zygotene stage of meiosis. Concurrently, the formation of the blood-testis barrier (BTB) was impaired in *Cep215* KO testes. These findings suggest that BTB failure contributes, at least partially, to male germ cell defects observed in *Cep215* KO mice. We propose that the deletion of *Cep215* may disrupt microtubule organization in Sertoli cells with a delay in spermatogonial stem cell mitosis, thereby impeding proper BTB formation.

**Abbreviations:** AKAP9, a-kinase anchoring protein 9; an, Hertwig's anemia; ANOVA, analysis of variance; BSA, bovine serum albumin; BTB, blood–testis barrier; Cas9, CRISPR-associated protein 9; Cdk5rap2, cyclin-dependent kinase 5 regulatory subunit associated protein 2; Cep215, centrosome protein 215; CM1, centrosomin motif 1; CRISPR, clustered regularly interspaced short palindromic repeats; DAB, 3,3'-diaminobenzidine; DAPI, 4',6-diamidino-2-phenylindole; DMEM, Dulbecco's modified eagle medium; DTT, dithiothreitol; EUCOMM, European conditional mouse mutagenesis program; FBS, fetal bovine serum; Gapdh, glyceraldehyde 3-phosphate dehydrogenase; H&E, hematoxylin and eosin; HSD3 $\beta$ , 3 $\beta$ -hydroxysteroid dehydrogenase; IgG-HRP, immunoglobulin G-horseradish peroxidase; KO, knockout; LacZ,  $\beta$ -galactosidase; MCPH3, autosomal recessive primary microcephaly type 3; P7, postnatal day 7; PBST, phosphate-buffered saline with 0.1% Triton X-100; PCM, pericentriolar material; PCR, polymerase chain reaction; RIPA, radio-immunoprecipitation assay; siRNA, small-interfering RNA; Sycp3, synaptonemal complex protein 3; TBST, Tris-buffered saline with 0.1% Tween 20; TdT, terminal deoxynucleotidyl transferase; Trp53, transformation-related protein 53; TUNEL, terminal deoxynucleotidyl transferase dUTP nick end labeling;  $\gamma$ H2AX, gamma H2A histone family member X.

This is an open access article under the terms of the [Creative Commons Attribution-NonCommercial](https://creativecommons.org/licenses/by-nc/4.0/) License, which permits use, distribution and reproduction in any medium, provided the original work is properly cited and is not used for commercial purposes.

© 2024 The Author(s). *The FASEB Journal* published by Wiley Periodicals LLC on behalf of Federation of American Societies for Experimental Biology.

## KEYWORDS

blood-testis barrier, Cep215/Cdk5rap2, male germ cells, meiosis, Sertoli cells, testis

## 1 | INTRODUCTION

Cep215/Cdk5rap2 stands out as a conserved centrosome protein crucial for microtubule organizing activity.<sup>1</sup> This protein comprises two distinct conserved domains: the CM1 domain, facilitating microtubule organization by interacting with the  $\gamma$ -tubulin ring complex, and the CM2 domain, responsible for centrosome localization through interactions with centrosome-specific proteins like AKAP and pericentrin.<sup>2–4</sup> The significance of microtubule organization orchestrated by Cep215 cannot be overstated, particularly in mitosis. Without Cep215, the proper formation of mitotic spindles is compromised, leading to mitotic delay.<sup>5–7</sup> Moreover, evidence suggests that Cep215 works beyond the centrosome, as its CM2 domain interacts with proteins located outside the centrosomes, such as those within the nuclear membrane and Golgi apparatus.<sup>8</sup>

*Cep215* serves as a causal gene implicated in autosomal recessive primary microcephaly type 3 (MCPH3), a prenatal neurodevelopmental disorder characterized by reduced small brain size and a thin cerebral cortex.<sup>9,10</sup> Patients with MCPH3 also commonly present with sensorineural hearing loss, abnormal skin pigmentation, and ocular defects.<sup>11–13</sup>

Four distinct mouse mutants associated with *Cep215* have been documented. The *Hertwig's anemia (an)* mutant, arising from the progeny of a heavily irradiated male mouse, displays an in-frame 111 bp deletion, leading to the loss of exon 4 of the *Cep215* gene.<sup>14–16</sup> *Cep215<sup>an/an</sup>* mice exhibit characteristic microcephalic features, mirroring observations in human microcephalic patients, alongside pleiotropic phenotypes affecting various tissues, including eyes, blood cells and male germ cells.<sup>16–19</sup> In another investigation, two splice-trap mutations, resulting in 64 and 435 amino acid truncations, designated *Cep215<sup>RRU031</sup>* and *Cep215<sup>RRF465</sup>*, respectively, were similar to the human *Cep215* mutations for MCPH3.<sup>9</sup> However, neither mutant displayed microcephaly nor other obvious defects in brain development.<sup>20</sup> Lastly, EUCOMM generated *Cep215<sup>tm1a</sup>* mice with a deletion in exon 5 of *Cep215*, yielding a LacZ-tagged null allele.<sup>21</sup> *Cep215<sup>tm1a</sup>* mice exhibit mild macrocytic normochromic anemia alongside abnormal head morphology.<sup>21,22</sup>

While male sterility has not been reported in MCPH3 patients, the testicular function is severely compromised

in the *Cep215<sup>an/an</sup>* mouse strain.<sup>17</sup> Male germ cells reside within seminiferous tubules alongside Sertoli cells, specialized somatic nursing cells. Sertoli cells exhibit an amorphous morphology, filling the interstitial space among germ cells while maintaining close contact with them at various developmental stages, albeit with strict polarity.<sup>23</sup> Critical to male reproductive physiology, Sertoli cells establish and maintain the blood-testis barrier (BTB), which segregates seminiferous tubules into the basal and adluminal compartments. Within the basal compartment, Sertoli cells anchor to the basement membrane of seminiferous tubules and interact with spermatogonia, thereby supporting the stem cell population.<sup>24</sup> Upon initiation of spermatogonial differentiation into spermatocytes, cells transition to the adluminal compartment, where they undergo meiosis and further maturation into spermatozoa.<sup>25</sup> Consequently, Sertoli cells play a pivotal role in orchestrating successful progression throughout male germ cell development.

In this study, we examined the phenotypes of a novel *Cep215*-deficient mouse model, where the majority of the *Cep215* locus was removed, thereby eliminating concerns regarding alternatively spliced variants. Our focus particularly centered on the testis phenotypes observed in our *Cep215* KO mice.

## 2 | MATERIALS AND METHODS

### 2.1 | Animals

The animal experiments in this study were permitted by the Institutional Animal Care and Use Committees at Asan Institute for Life Sciences (Approval number: 2021-12-185) and at Seoul National University (SNU-211112-3). All mice were maintained in the specific pathogen-free facility of the Laboratory of Animal Research at Asan Medical Center. To establish the *Cep215* KO mouse model using the CRISPR/Cas9 system, mouse *Cep215* genomic DNA sequence (NC\_000070.7: 70135092.70328672) was analyzed using Snapgene software from GSL Biotech (Boston, USA), and guide RNA sequences were designed using a web-based software ([Benchling.com](http://Benchling.com)). Four guide RNA sequences specific for the introns 1 (LRG3 and LRG4) and 34 (RRG11 and RRG12) were cloned into *pUC57-sgRNA* vector (Addgene plasmid #51132) according to the manual,<sup>26</sup> and then these plasmids were used as

templates for the *in vitro* transcription of the guide RNAs as previously described.<sup>27</sup> The oligomers that are listed in [Figure 1A](#) were used for the cloning after annealing.

For mutant mice generation, C57BL/6NTac (B6N) as embryo donors and ICR mice as foster mothers were purchased from OrientBio Inc. (Seongnam, Korea) and DBL Co. Ltd. (Chungbuk, Korea), respectively, and were prepared as previously reported.<sup>28</sup> For efficient gene targeting, four guide RNAs were simultaneously applied. Based on a previous report,<sup>29</sup> 50 ng/ $\mu$ L recombinant Cas9 protein (M0386T) from New England Biolabs and 200 ng/ $\mu$ L guide RNAs specific for introns 1 and 34 of the mouse *Cep215* gene in Opti-MEM (Thermo Fisher Scientific) were delivered into mouse zygotes by electroporation using the Super Electroporator NEPA 21 (NEPA GENE, Chiba, Japan). The manipulated mouse embryos were transferred into the oviduct ampulla of pseudo-pregnant foster mothers.

We utilized three PCR primers for genotyping deletions of the *Cep215* gene ([Table 1](#)). The common forward primer binds to intron 1, upstream of the gRNA targeting site. To detect the wild-type allele, we used a reverse primer which binds to intron 1, downstream of the gRNA targeting site. For detection of the KO allele, we used a second reverse primer which binds to intron 34, downstream of the 3' end gene deletion site. As a result, the PCR products of the wild-type and KO alleles are 621 and 569 bp in size, respectively ([Figure 1B](#)).

The generation of *Trp53* KO mouse was previously reported,<sup>28</sup> and we used a mutant mouse line harboring a 25-bp deletion corresponding to nucleotides 747–771 of the *Trp53* mRNA (NM\_011640.4) encoding amino acids 212–220 of the mouse Trp53 protein (NP\_035770.2). The mutant alleles were verified by Sanger sequencing, and PCR genotyping strategies were set up for the routine mouse colony management ([Table 1](#)). Tissues were acquired after euthanasia using CO<sub>2</sub> and perfused with PBS.

## 2.2 | Antibodies

The *Cep215* and *Pcnt* antibodies were previously described.<sup>5,30</sup> The antibodies were commercially purchased as listed below: *Cep215* (06-1398; Millipore),  $\gamma$ H2AX (05-636; Upstate), *Sycp3* (ab15093; Abcam), *centrin-2* (04-1624; Millipore),  $\gamma$ -tubulin (ab11316-100; Abcam),  $\gamma$ -tubulin (ab11317; Abcam), *claudin-11* (36-4500; Invitrogen), *connexin43* (3512; Cell signaling), *Sox9* (AB5535; Millipore), *vimentin* (ab92547; Abcam), *Gapdh* (AM4300; Invitrogen), and *HSD3 $\beta$*  (GTX102744; Genetex). The Alexa-fluorescence secondary antibodies were purchased from Invitrogen. The mouse and rabbit IgG-HRP antibodies were purchased from Sigma and Millipore, respectively.

## 2.3 | Immunoblot analyses

The perfused mouse organs were homogenized in RIPA buffer (150 mM NaCl, 1% Triton X-100, 0.5% sodium deoxycholate, 0.1% SDS, 50 mM Tris-HCl at pH 8.0, 10 mM NaF, 1 mM Na<sub>3</sub>VO<sub>4</sub>, 1 mM EDTA and 1 mM EGTA) containing a protease inhibitor cocktail (P8340; Sigma-Aldrich) and placed on ice for 10 min. The tissue lysates were centrifuged at 12000 rpm for 10 min at 4°C. The supernatants were mixed with 4 $\times$ SDS sample buffer (250 mM Tris-HCl at pH 6.8, 8% SDS, 40% glycerol, 400 mM DTT, and 0.04% bromophenol blue), boiled for 5 min, and subjected to SDS-polyacrylamide gel electrophoresis. Proteins in the gel were transferred to a nitrocellulose membrane. The membrane was blocked with 5% skimmed milk in 0.1% TBST (Tris-buffered saline TBS with 0.1% Tween 20) for 1–2 h, incubated with the primary antibodies overnight at 4°C, and with horseradish peroxidase-conjugated secondary antibody for 30–40 min at room temperature, treated with the ECL solution, and then exposed to X-ray films.

## 2.4 | H&E staining

Dissected mouse tissues were fixed in 4% paraformaldehyde solution or Bouin's solution (HT10132; Sigma) overnight at 4°C. After washing, the fixed tissues were embedded in paraffin and sectioned with 3  $\mu$ m thickness in case of testis or 5  $\mu$ m thickness in case of brain. The sectioned samples were subjected to histological analysis, immunohistochemistry, and TUNEL assay. For the histological analyses, hematoxylin and eosin staining was carried out, using an automatic staining machine (Leica ST5010 Autostainer XL). Images of H&E staining were acquired from the light microscope (Olympus BX 51) and processed with ProgRes<sup>®</sup> CapturePro (Jenoptik).

## 2.5 | Immunohistochemistry

The testis sections were rehydrated and boiled for 25 min in antigen retrieval buffers, such as the citrate buffer (pH 6.0) or the Tris-EDTA buffer (pH 9.0), depending on the primary antibodies. The tissues were permeabilized with 0.1% PBST (phosphate-buffered saline with 0.1% Triton X-100) for 10 min, blocked with 3% bovine serum albumin (BSA) in 0.5% PBST for 30 min, and incubated with the primary antibodies overnight at 4°C. After washing with 0.1% PBST three times, the tissues were incubated with the secondary antibodies for 30–45 min, washed with 0.1% PBST three times, and mounted with cover glass using Prolong gold mounting solution (Invitrogen) after DAPI

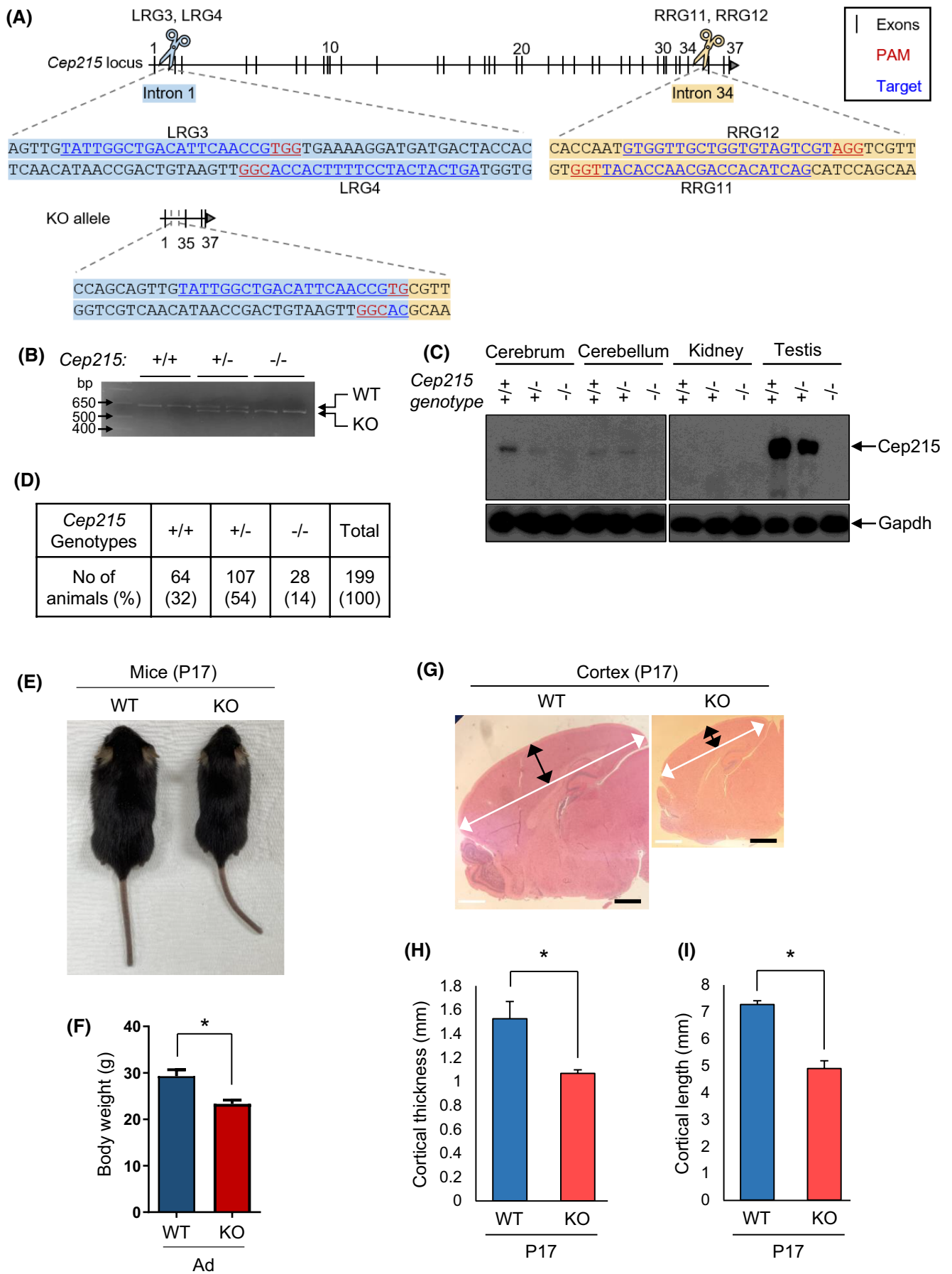


**FIGURE 1** Generation of the *Cep215* total KO mouse. (A) Summary of a total deletion of the *Cep215* gene using the CRISPR-Cas9 system. The guide RNAs targeted introns 1 and 34, resulting in a deletion of 175 kb from exons 2–34 of the *Cep215* gene. (B) PCR genotyping of the *Cep215* KO mice. (C) Immunoblot analyses of the tissues from adult *Cep215* KO mice with *Cep215* and *Gapdh* antibodies. (D) The number of progenies from *Cep215* heterozygote matings. (E) *Cep215* KO and littermate (WT) mice at P17. (F) The body weights of the adult *Cep215* KO and littermate (WT) mice. (G–I) H&E staining of the whole brain of *Cep215* KO mice at P17. The cortical thickness (black arrows) and the length (white arrows) of the brain (G) were marked. Scale bars: 1 mm. The cortical thickness (H) and the length (I) of the brains were measured. (F, H, I) Values are means and SEM ( $n = 3$ ). The statistical significance was determined by unpaired *t*-test. \* $p < .05$ .

**TABLE 1** PCR primers for genotyping.

Genes	Primers	Sequences	Size
<i>Cep215</i>	<i>Cep215</i> #F (common)	5'-CGATGTGTAGGCTAGGCAGG-3'	WT: 621 bp
	<i>Cep215</i> #R1 (WT-specific)	5'-TCCTGAAGATGACAAGGCACC-3'	KO: 569 bp
	<i>Cep215</i> #R2 (KO-specific)	5'-ATGCCCTTCCCCAGAACAG-3'	
<i>Trp53</i>	<i>Trp53</i> #F	5'-CGCCATGGCCATCTACAAGA-3'	WT: 486 bp
	<i>Trp53</i> #R	5'-TCAGCGTCTCTATTTCCCGC-3'	KO: 461 bp

incubation. For triple staining, third antibodies were prepared with Zenon Alexa fluor labeling kit following the protocol of the manufacturer, and the tissues were incubated with conjugated antibodies for 2 h.

The immunostained tissues were observed using a fluorescence microscope with a CCD (CoolSNAP EZ CCD; Photometrics) camera and processed with PVCamtest (Photometrics), Adobe Photoshop software, and ImageJ software. For confocal images, the samples were observed using LSM 700 (Carl Zeiss), and the images were analyzed using ZEN lite software (Carl Zeiss).

To measure the centrosome levels of a specific protein, we quantified the intensities within 4- $\mu$ m-diameter circles encompassing the centrosomes. For background correction, we measured the intensities of the same circles in nearby the areas lacking centrosomes. The centrosome protein levels were calculated by subtracting the background signals from the intensity measured in the centrosome-containing circles.

For detection of Leydig cells, we detected the HSD3 $\beta$  signals with the 3,3'-diaminobenzidine (DAB) staining method applying Vectastain ABC-HRP kit (PK-4001; Vector Laboratories). To analyze the whole testes section, tile-scanning was conducted with EVOS FL Auto2 using 40 $\times$  (ThermoFisher).

## 2.6 | TUNEL assay

The TUNEL assay was performed using the FragEL™ DNA Fragmentation Detection Kit (Q1A39; Calbiochem), strictly following the manufacturer's instruction. In brief, the paraffin-embedded testis sections were rehydrated and permeabilized with proteinase K. The tissues were

treated with the terminal deoxynucleotidyl transferase (TdT) labeling mixture to mark exposed 3'-OH ends of DNA fragments formed during apoptosis, incubated in a humidified chamber at 37°C for 1.5 h and mounted using Fluorescein-FragEL™ Mounting Media. Labeled nuclei were visualized using a filter for 488 nm.

## 2.7 | Chromosome spreading analysis of male germ cells

Immunostaining analysis of chromosome spreading was performed following Gopinathan et al.<sup>31</sup> with minor modifications. In brief, the testes were excised and placed in PBS. The tunica albuginea was carefully removed and the seminiferous tubules were slightly teased apart with blunt forceps. The seminiferous tubules were incubated with hypotonic extraction buffer (30 mM Tris pH 8.2, 50 mM sucrose, 17 mM sodium citrate dihydrate, 5 mM EDTA) with inverting for 30 min to 1 h on ice depending on the size of testes. The seminiferous tubules were placed in a microtube with 250–1000  $\mu$ L of 100 mM sucrose pH 8.2 and pipetted repeatedly around 50 times until the solution turned cloudy. A poly-L-lysine coated slide was dipped in freshly prepared fixative solution (1% paraformaldehyde, 30 mM sodium tetraborate, 0.15% Triton X-100 in PBS), 50  $\mu$ L of the seminiferous tubule suspension was added and suspended a few times at the edge of the slide with droplets of fixative solution. The solution was allowed to spread along the length of the slide. The slides were placed in a humidified chamber for 6–7 h at 4°C, and stored at –20°C until used for immunostaining.

For immunostaining analysis, the slides with chromosome spreads were washed with PBS three times,

permeabilized with 0.1% PBST for 10 min, blocked with 3% BSA in 0.5% PBST for 1 h, and incubated with the primary antibodies overnight in humidified chamber at 4°C. After washing with 0.1% PBST three times, the slides were incubated with the secondary antibodies for 1 h, washed with 0.1% PBST three times, and mounted with a cover glass using Prolong gold mounting solution after DAPI incubation.

## 2.8 | Primary culture of Sertoli cells

Isolation and culture of primary Sertoli cells were performed following Ahmadi et al.<sup>32</sup> with minor modifications. In brief, the 3-week-old mice were sacrificed and testes were placed in PBS. The tunica albuginea was removed carefully and the seminiferous tubules were slightly teased with blunt forceps. The tissue was digested first with prewarmed trypsin for 15 min and then with prewarmed 0.1% collagenase for another 15 min. After the sequential digestions, the cell suspension was spun down, suspended with Dulbecco's modified eagle medium with 10% fetal bovine serum (DMEM with 10% FBS), and seeded on coverslips. Two days later, the medium was changed and 40 nM siRNA was transfected using Lipofectamine RNAiMAX (Cat. No. 13778075; Invitrogen) and cultured further for 48 h before fixation with cold methanol for immunostaining. The siRNAs specific to mouse *Cep215* (5'-GAG AUC ACC UUG AUA GUA ATT-3')<sup>33</sup> and non-specific control siRNA (5'-GCA AUC GAA GCU CGG CUA CTT-3') were purchased from Cosmogenetech.

For immunostaining analysis, the coverslips were washed with PBS three times, permeabilized with 0.1% PBST for 10 min, blocked with 3% BSA in 0.5% PBST for 30 min, and incubated with primary antibodies 1 h at room temperature. After washing with 0.1% PBST for three times, the cells were incubated with secondary antibodies for 30 min, washed with 0.1% PBST 3 times, and mounted using a Prolong gold mounting solution after DAPI incubation. The immunostained cells were observed and processed in the same manner as described in the Immunohistochemistry section.

## 2.9 | Biotin trace assay

The mice were sacrificed, and testes were dissected. The testes were injected with 50  $\mu$ L EZ-Link Sulfo-NHS-LC-Biotin (10 mg/mL in 1 mM CaCl<sub>2</sub>; #21335; Thermo Fisher Scientific), incubated in DMEM with 10% FBS for 30 min at 37°C, fixed in Bouin's solution overnight, and embedded in a paraffin block. The testicular tissue was sectioned at 3  $\mu$ m thickness, rehydrated, blocked with

3% BSA in 0.5% PBST for 30 min, and incubated with Alexa Fluor 488-conjugated streptavidin (1:200, #S32354; Invitrogen) for 40 min at room temperature to visualize the biotin signals.

## 2.10 | Statistical analyses

For statistical analyses, experiments were independently performed three times. To calculate *p* values, all data were analyzed using the Prism 8 software (GraphPad Software) including unpaired two-tailed *t*-test, one- or two-way analysis of variant (ANOVA). In the case of ANOVA, Tukey's posttest or Sidak's posttest were performed if the *p* values were lower than .05. Fluorescent intensities were displayed with box-and-whiskers plots in Prism 8 (lines, median; vertical boxes, values from 25th and 75th; down error bars, 5th value, up error bar, 95th value; circle, outliers).

## 3 | RESULTS

### 3.1 | Generation of the *Cep215* total KO mouse

Previous efforts to generate *Cep215* KO mice resulted in small deletions at early exons, potentially allowing the persistence of alternative splicing variants of *Cep215* in cells.<sup>20,34</sup> To overcome this limitation and eliminate potential interference from residual *Cep215* variants, we engineered novel *Cep215* KO mice in which the majority of the *Cep215* locus was excised. Complete deletion of the *Cep215* gene was accomplished using a CRISPR-Cas9 system simultaneously targeting introns 1 and 34, as confirmed by PCR genotyping (Figure 1A,B). Immunoblot analyses revealed that *Cep215* was predominantly expressed in the testis and also detected in the brain (cerebrum and cerebellum), with minimal expression in the kidney (Figure 1C). Notably, no specific band corresponding to *Cep215* was observed in any tissues of the *Cep215* KO mice, confirming the successful elimination of the *Cep215* gene (Figure 1C).

Progeny homozygous for the *Cep215* mutant allele were born at a lower frequency than expected, suggesting potential embryonic lethality associated with the total deletion of *Cep215* (Figure 1D). However, surviving homozygote mice displayed small body sizes and blunt facial features, without experiencing early postnatal mortality (Figure 1E,F). Of particular note, cortical thickness and length were significantly reduced in *Cep215* KO mice, indicative of microcephaly (Figure 1G-I). These observations closely resemble the phenotypic traits observed in *Cep215*<sup>an/an</sup> mice.<sup>16</sup>

### 3.2 | Histological analysis of the developing testes in *Cep215* KO mice

The *Cep215<sup>an/an</sup>* mouse exhibits a spectrum of phenotypes, encompassing microcephaly, anemia, eye malformation, and prominently, male sterility.<sup>16–19</sup> Consistent with these observations, we noted reduced testicular volumes in our *Cep215* KO mice (Figure 2A,B). Given that mouse spermatogenesis commences at P10 and progresses to meiosis by P17, we conducted analyses at P7, P17, and in adult mice to evaluate male germ cell development.<sup>35,36</sup> At P7, the area of seminiferous tubules in both wild-type and KO testes were approximately identical and P7 testes prominently consisted of Sertoli cells and spermatogonia (Figure 2C,D). P17 testes additionally contained spermatocytes, but a notable reduction in meiotic germ cells was observed (Figure 2C,D). The average area of seminiferous

tubules in *Cep215* KO testes at P17 was roughly half of the wild-type testes, likely due to reduced numbers of germ cells (Figure 2C,D). The postmeiotic germ cells were absent in adult *Cep215* KO mice (Figure 2C,D). These findings indicate that while male germ cells in *Cep215* KO testes may initiate differentiation into premeiotic spermatocytes, they fail to complete through meiosis.

### 3.3 | The numbers of Sertoli and Leydig cells are not affected by *Cep215* KO

Deletion of *Cep215* is known to disrupt mitotic spindle formation, resulting in mitotic delay. To investigate whether *Cep215* deletion affects the proliferation of testicular cells, we quantified the number of testicular cells in immature testes of *Cep215* KO mice. We quantified the numbers of

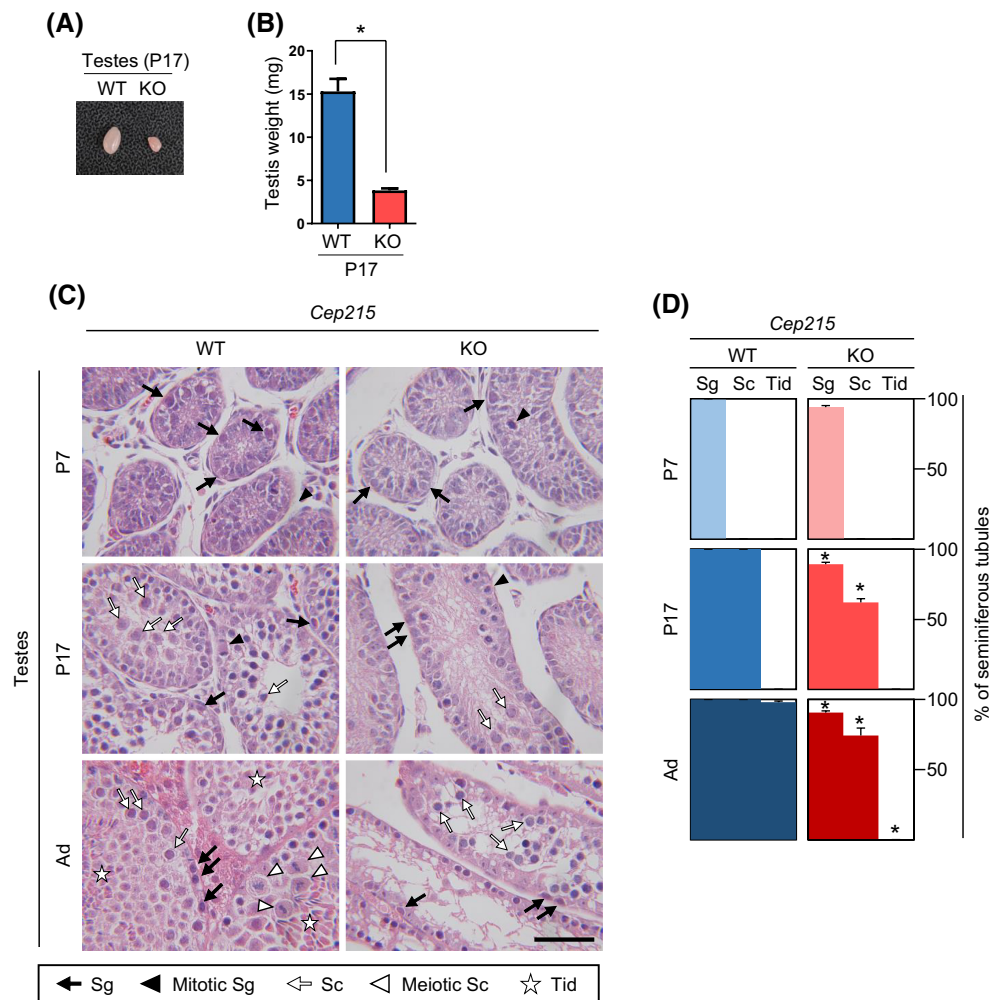


**FIGURE 2** Histological analysis of the *Cep215* KO testes. (A) Testes of the *Cep215* KO and littermate (WT) mice at P17. (B) Weights of the testes from the *Cep215* KO mice at P17. (C) H&E staining of the testes from *Cep215* KO mice at P7, P17, and adult. Scale bars: 50  $\mu$ m. (D) The number of seminiferous tubules with spermatogonia (Sg), spermatocytes (Sc), and spermatids (Tid) was counted. At least 200 tubules per experimental group were analyzed ( $n=3$ ). (B, D) Values are means and SEM. The statistical significance was determined by unpaired *t*-test (B) or two-way ANOVA (D). \* $p < .05$ .

germ and Sertoli cells in seminiferous tubules with circular morphology, excluding those with oblique sections. In wild-type testes, the number of male germ cells exhibited a dramatic increase during early development. However, in *Cep215* KO testes, the number of male germ cells was significantly reduced at both P7 and P17 (Figure 3A,B). These findings suggest that spermatogonial stem cells proliferate less actively in the absence of *Cep215*. Interestingly, the number of Sertoli cells remains similar between the wild-type and *Cep215* KO testes, suggesting that *Cep215* has minimal effects on the proliferation of Sertoli cells during the early developmental stage (Figure 3A,B).

We also quantified the number of Leydig cells in testis sections using HSD3 $\beta$  as a marker.<sup>37</sup> As expected, the cross-section area of wild-type testes increased significantly, particularly in adulthood, whereas *Cep215* KO testes showed only a slight increase, likely due to the absence of postmeiotic germ cells (Figure 3C,D). Correspondingly, Leydig cell numbers increased in both wild-type and *Cep215* KO testes. In contrast, no significant difference in Leydig cell numbers counted per cross section was observed between the wild-type and mutant testes at immature stage, despite the fact that wild-type testis at P17 were roughly twice larger than those of *Cep215* KO mice (Figure 3C,D). These findings

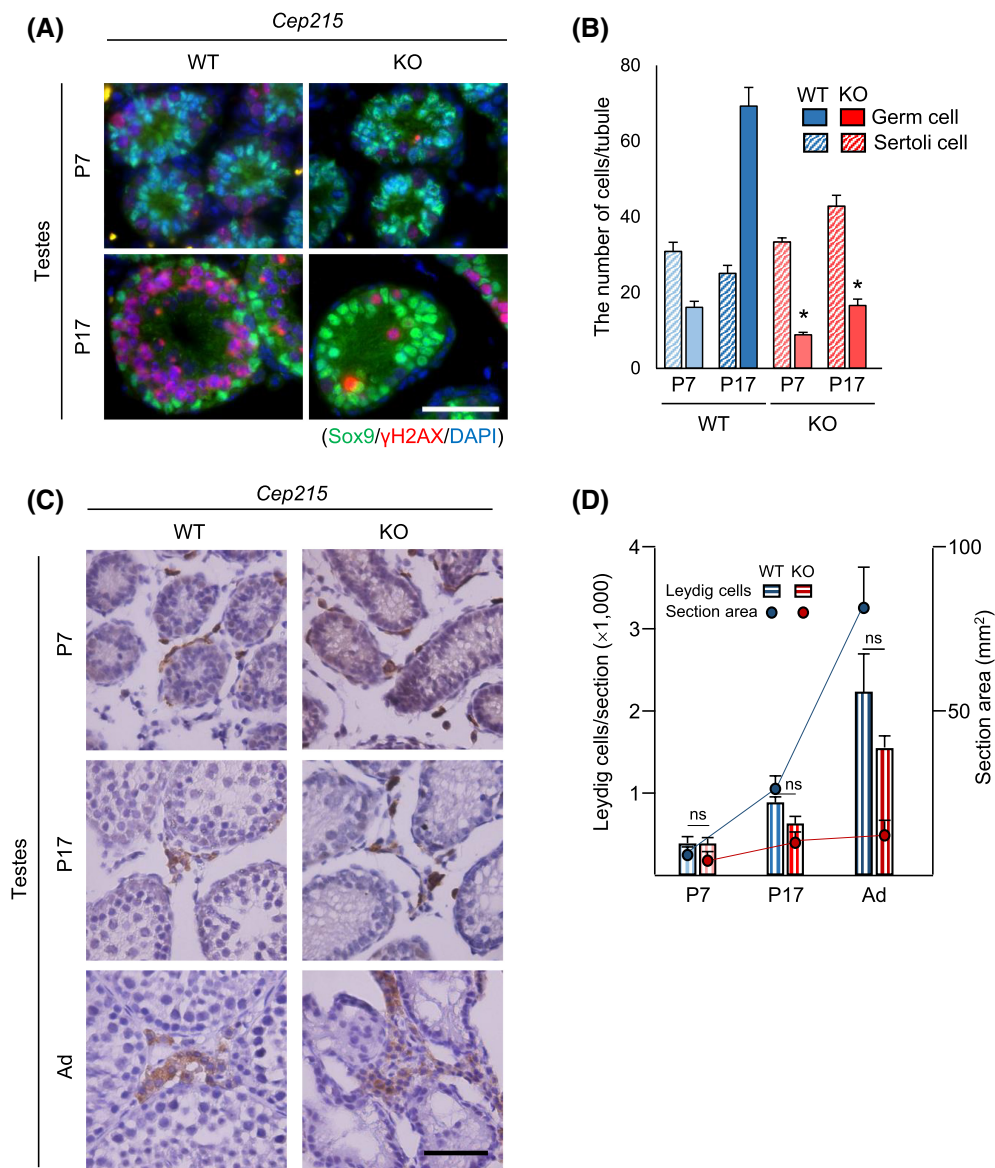


**FIGURE 3** The numbers of germ, Sertoli, and Leydig cells in *Cep215* KO testes. (A) Immunohistochemistry of the testes from *Cep215* KO mice at P7 and P17 with Sox9 (green) and  $\gamma$ H2AX (red) antibodies. (B) The number of Sertoli and germ cells per tubule was counted. At least 1200 cells per experimental group were counted ( $n = 3$ ). (C) Immunohistochemistry of the testes from *Cep215* KO mice at P7, P17, and adult with HSD3 $\beta$  antibody. (D) The number of Leydig cells per section was counted (bars). The cross-sectional area was also measured (dots). At least 90 cells per section were counted ( $n = 3$ ). (A, C) Scale bars: 50  $\mu$ m. (B, D) Values are means and SEM. The statistical significance was determined by two-way ANOVA (B) and unpaired  $t$ -test (D). \* $p < .05$ . ns, not significant.



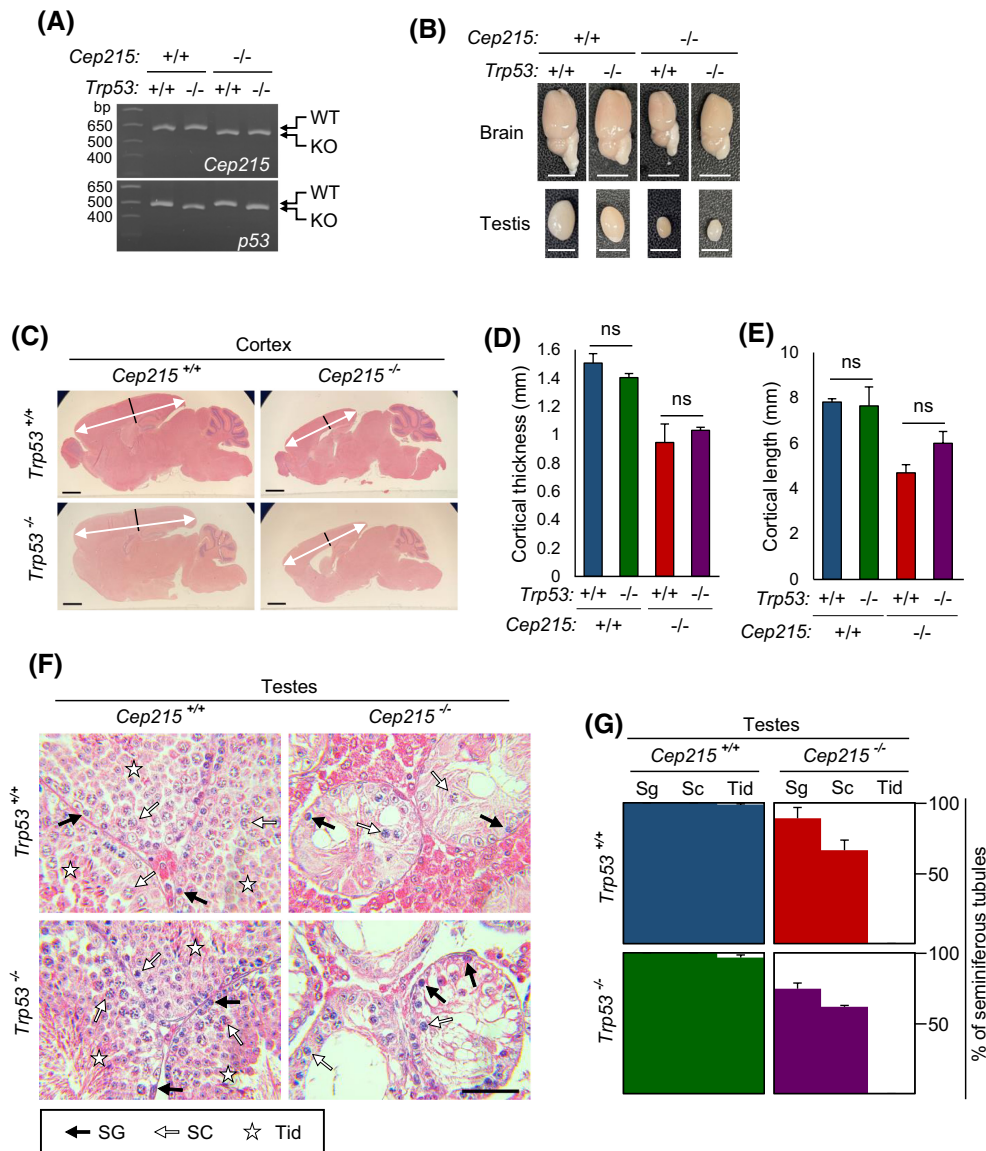
suggest that serum testosterone levels may be similar between wild-type and *Cep215* KO mice at immature stages.

### 3.4 | Phenotypes of the *Cep215;Trp53* double KO mice

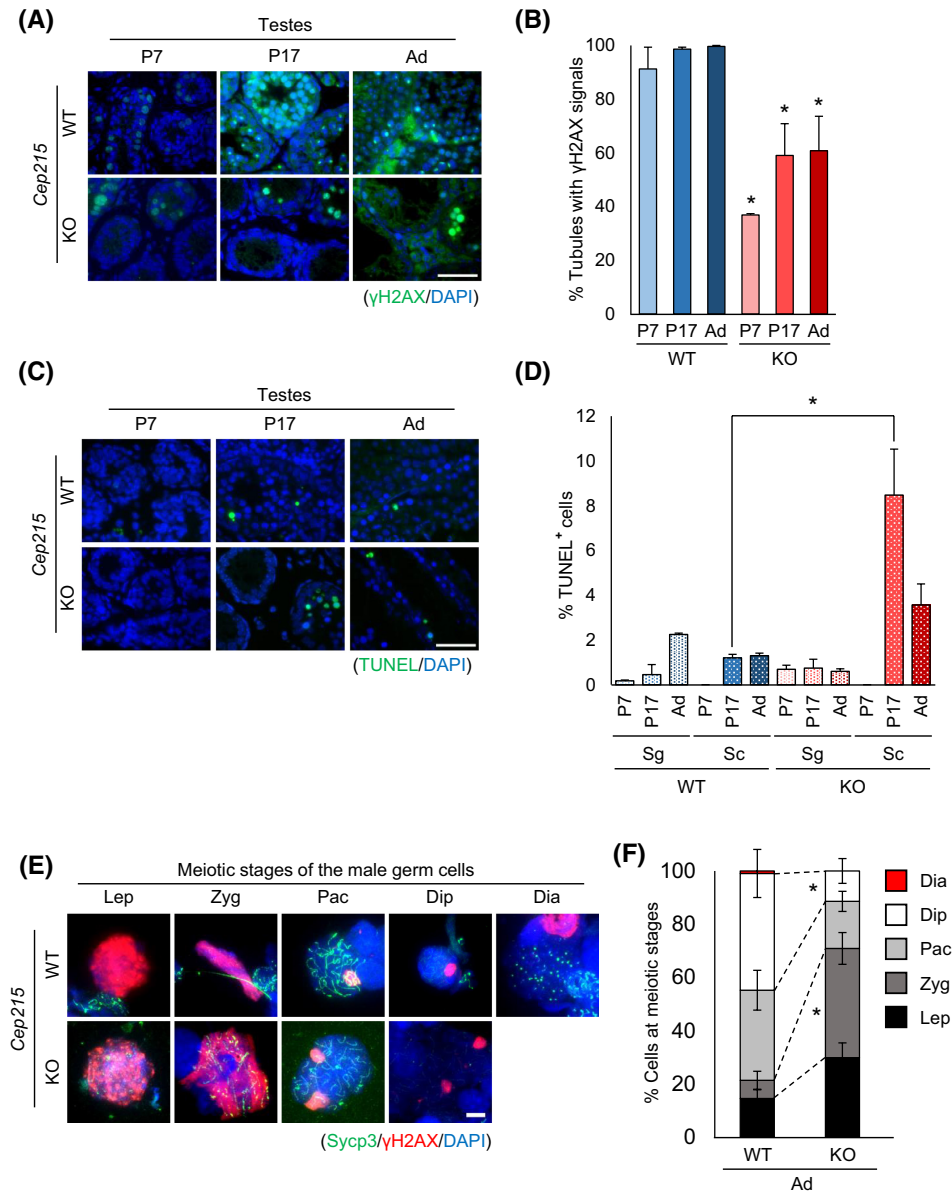
Deletions of centrosome genes often lead to organs with diminished cell numbers and of reduced sizes.<sup>38</sup> This phenotype is frequently accompanied by extensive apoptosis in the KO tissues and preventing apoptosis may alleviate the severity of these phenotypes in some cases. For

example, the *Sas4/Cpap* KO mice are embryonic lethal at E13 with reduced brain sizes.<sup>39</sup> Additional deletion of *Trp53*, resulting in double KO (dKO) of *Cpap* and *Trp53*, partially rescues the lethal phenotypes of the *Cpap* KO brains, suggesting that *Cpap* KO induces p53-dependent apoptosis in brain cells.<sup>39</sup> Therefore, we investigated the general phenotypes of *Cep215;Trp53* dKO mice to determine whether p53-dependent apoptosis contributes to the typical phenotypes observed in *Cep215* KO mice, such as microcephaly and male infertility.

We confirmed the gene deletion by genotyping PCR (Figure 4A). Brain and testis sizes of *Trp53* KO mice were

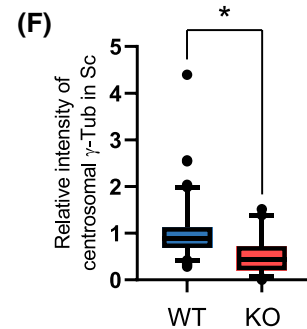
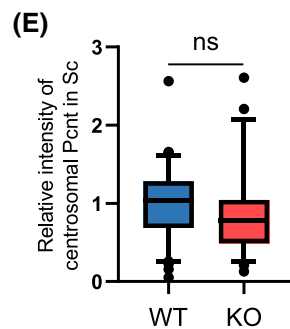
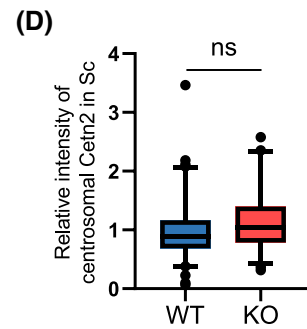
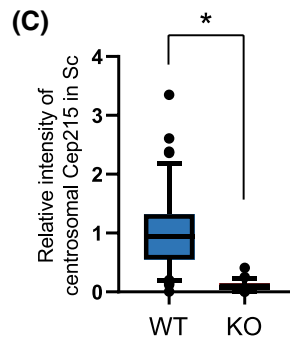
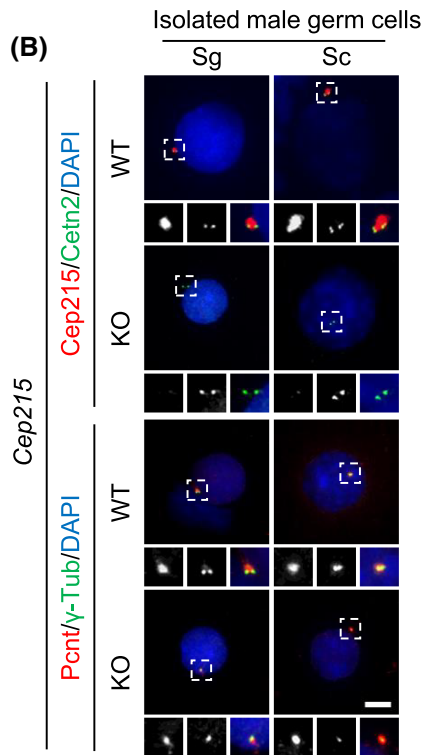
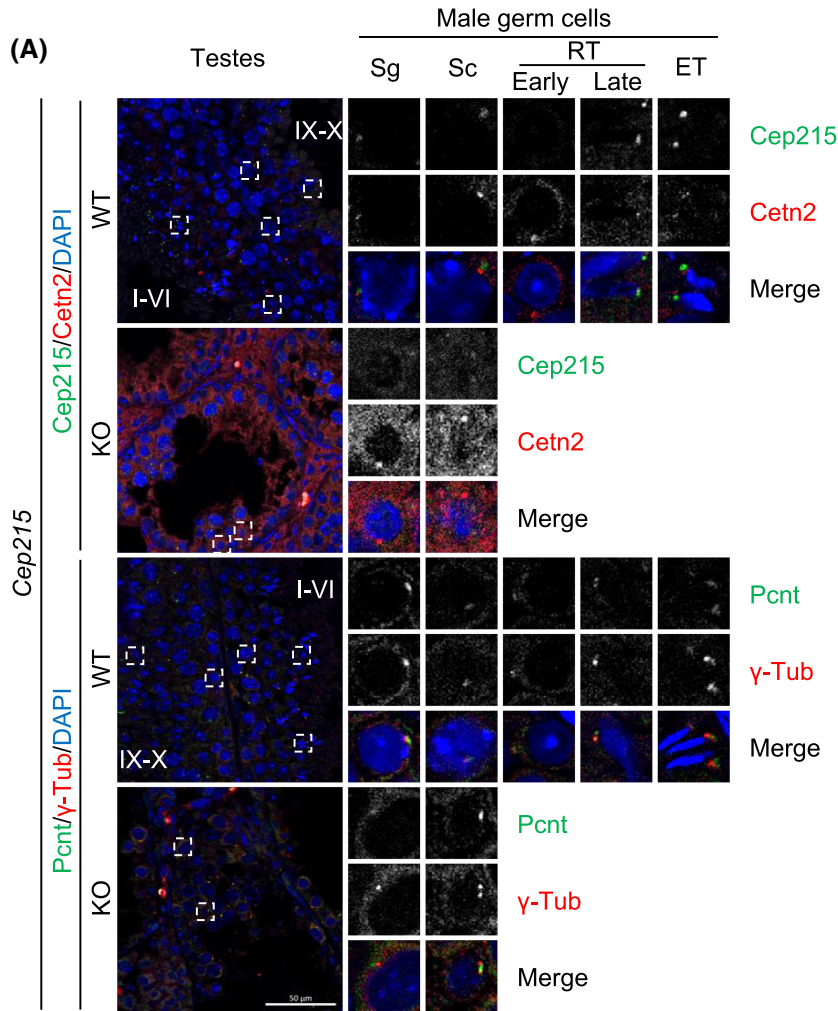


**FIGURE 4** Phenotypes of the *Cep215;Trp53* double KO mice. (A) Genomic PCR analyses for genotyping of the *Cep215;Trp53* double KO mice. (B) Brains and testes of the *Cep215;Trp53* double KO mice. Scale bars: 5 mm. (C) H&E staining of the brains from *Cep215;Trp53* double KO mice. The cortical thickness (black lines) and the length (white arrows) of the brain were marked. Scale bar, 1 mm. (D, E) The cortical thickness (D) and length (E) of the brains were measured. (F) H&E staining of the testes from adult *Cep215;Trp53* double KO mice. Scale bar, 50 μm. (G) The number of seminiferous tubules with spermatogonia (Sg), spermatocytes (Sc), and spermatids (Tid) was counted. At least 170 tubules per experimental group were analyzed in two mice. (D, E, G) Values are means and SEM. ns, not significant.



**FIGURE 5** Meiotic defects in the *Cep215* KO male germ cells. (A) Immunohistochemistry of the testes from *Cep215* KO mice at P7, P17, and adult with  $\gamma$ H2AX antibody (green). (B) The number of tubules with  $\gamma$ H2AX-positive meiotic cells was counted. At least 220 tubules per experimental group were counted. (C) TUNEL assays with the testes of *Cep215* KO mice at P7, P17, and adult. (D) The number of TUNEL-positive spermatogonia (Sg) and spermatocytes (Sc) was counted. At least 1000 cells per experimental group were counted. (E) Co-immunostaining of the spermatocytes isolated from the testes of adult *Cep215* KO mice with the Sycp3 (green) and  $\gamma$ H2AX (red) antibodies. Meiotic stages were determined based on the immunostaining patterns. Scale bars: 10  $\mu$ m. (F) The number of spermatocytes at specific meiotic stages was counted. At least 270 cells per experimental group were counted ( $n = 3$ ). (A, C, E) Nuclei were stained with DAPI (blue). (A, C) Scale bars, 50  $\mu$ m. (B, D, F) Values are means and SEM. The statistical significance was determined by two-way ANOVA. \* $p < .05$ , compared to the wild type groups.

**FIGURE 6** Centrosomes in the *Cep215* KO male germ cells. (A) Immunohistochemistry of the *Cep215* KO testes with Cep215 (green), centrin-2 (red), Pcnt (green), and  $\gamma$ -tubulin (red) antibodies. Inlets are enlarged views of the male germ cells at specific developmental stages (Sg, spermatogonia; Sc, spermatocyte; RT, round spermatid; ET, elongated spermatid). Scale bars, 50  $\mu$ m. (B) Immunostaining of the isolated spermatogonia and spermatocytes from *Cep215* KO testes with Cep215 (red), centrin-2 (green), Pcnt (red) and  $\gamma$ -tubulin (green) antibodies. Scale bars, 10  $\mu$ m. (A, B) Nuclei were stained with DAPI (blue). (C–F) Centrosome intensities of Cep215 (C), centrin-2 (D), Pcnt (E), and  $\gamma$ -tubulin (F) in the *Cep215* KO spermatocytes at P17. At least 50 cells per experimental group were counted ( $n = 3$ ). Fluorescent intensities were displayed with box-and-whiskers plots (lines, median; vertical boxes, values from 25th and 75th; down error bars, 5th value, up error bar, 95th value; circle, outliers). The statistical significance was determined by an unpaired *t*-test. \* $p < 0.05$ . ns, not significant.



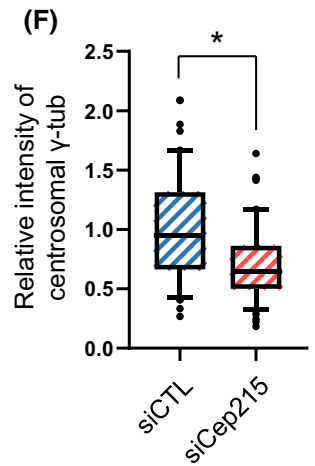
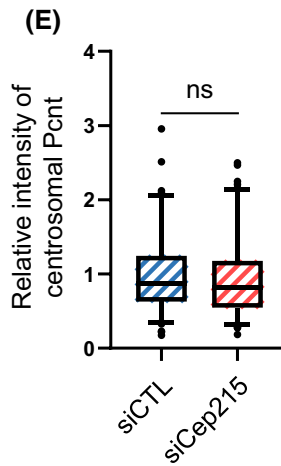
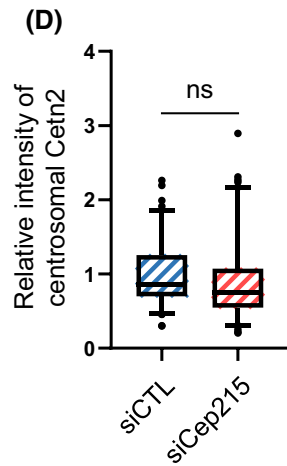
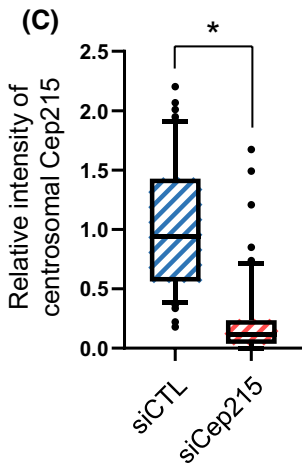
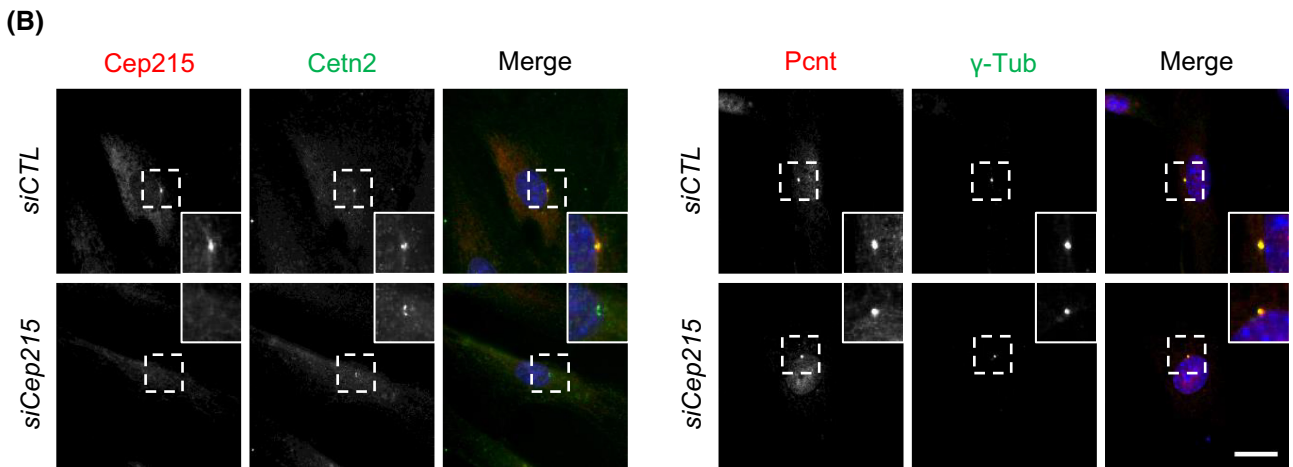
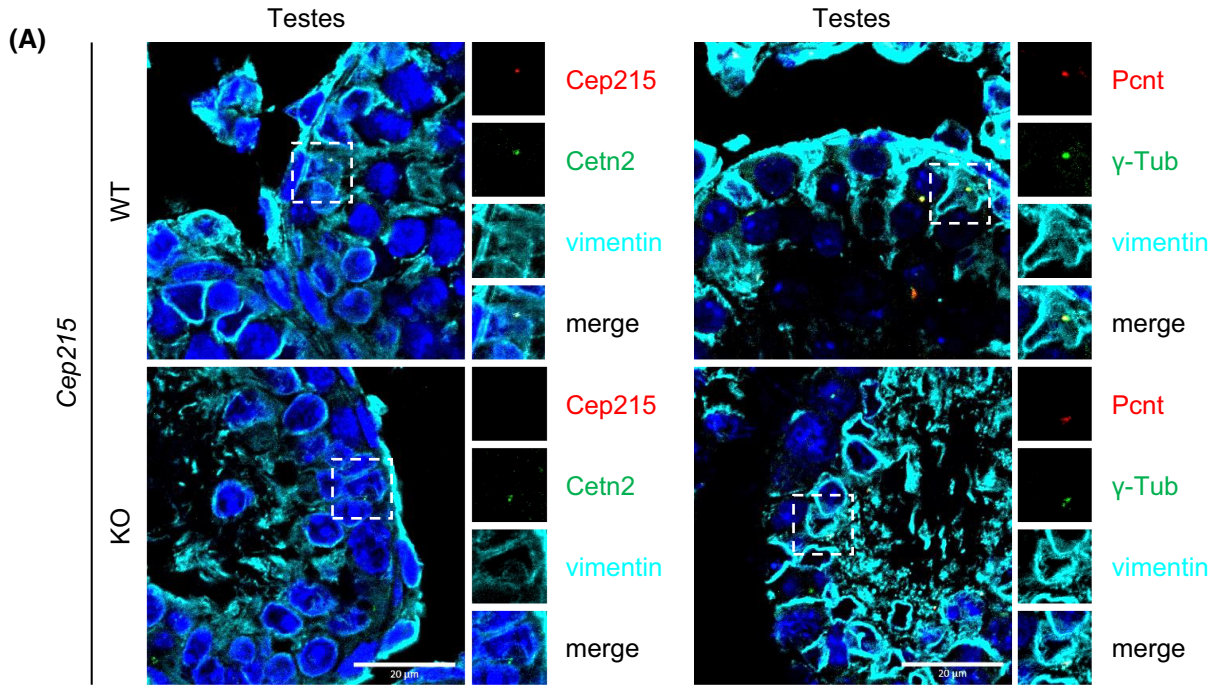


**FIGURE 7** Centrosomes in the *Cep215* KO Sertoli cells. (A) Immunohistochemistry of the *Cep215* KO testes at P17 with Cep215 (red), centrin-2 (green), Pcnt (red),  $\gamma$ -tubulin (green), and vimentin (cyan) antibodies. Inlets are enlarged views of the Sertoli cells marked with the vimentin antibody. (B) Immunostaining of the isolated Sertoli cells with the Cep215 (red), centrin-2 (green), Pcnt (red), and  $\gamma$ -tubulin (green) antibodies. (A, B) Nuclei were stained with DAPI (blue). Scale bars: 20  $\mu$ m. (C–F) Centrosomal intensities of Cep215 (C), centrin-2 (D), Pcnt (E), and  $\gamma$ -tubulin (F) in Sertoli cells. At least 100 cells per experimental group were counted ( $n = 3$ ). Fluorescent intensities were displayed with box-and-whiskers plots (lines, median; vertical boxes, values from 25th and 75th; down error bars, 5th value, up error bar, 95th value; circle, outliers). The statistical significance was determined by an unpaired *t*-test. \* $p < .05$ . ns, not significant.

normal, whereas those of *Cep215;Trp53* dKO mice are as small as the *Cep215* KO mice (Figure 4B). Histological analysis of brain tissue via H&E staining revealed that *Cep215;Trp53* dKO mice exhibited reduced cortical thickness and length, similar to *Cep215* KO mice (Figure 4C–E). These results indicate that the microcephaly caused by *Cep215* mutations was not alleviated by concurrent deletion of *Trp53*. Similarly, seminiferous tubules in *Cep215;Trp53* dKO testes lacked postmeiotic germ cells, akin to observations in *Cep215* KO testes (Figure 4F,G). The results suggest that p53-dependent cell death may not be implicated in the developmental defects of the brain and testes in *Cep215* KO mice.

### 3.5 | Defects in *Cep215* KO spermatocytes

While spermatocytes were present in the *Cep215* KO testes, their numbers were notably diminished compared to those in littermate testes. This observation hints at a potential impairment in the meiotic progression of *Cep215* KO male germ cells. Indeed, a significant proportion of seminiferous tubules lacked  $\gamma$ H2AX-positive meiotic germ cells in *Cep215* KO testes (Figure 5A,B). Furthermore, some seminiferous tubules were devoid of any germ cells at all in *Cep215* KO testes, suggesting that male germ cells in *Cep215* KO mice might undergo apoptosis during meiotic prophase. To investigate further, we conducted TUNEL assays to assess apoptosis in male germ cells of *Cep215* KO testes. The results revealed that premeiotic male germ cells in *Cep215* KO mice undergo apoptosis more frequently than those in wild-type mice (Figure 5C,D). Notably, apoptosis was most prevalent at the spermatocyte stage (Figure 5D), suggesting that the development of male germ cells in *Cep215* KO mice is arrested at meiotic prophase and subsequently eliminated via apoptosis.

To pinpoint specific stages of meiotic prophase at which apoptosis occurs in *Cep215* KO male germ cells, we isolated spermatocytes from the wild-type and *Cep215* KO testes and coimmunostained with Sycp3 and  $\gamma$ H2AX antibodies (Figure 5E). In wild-type testes, the majority of primary spermatocytes were predominantly at the pachytene or diplotene stages (Figure 5F). Conversely, leptotene and zygotene spermatocytes were more prevalent in *Cep215*

KO testes, with a reduction of the pachytene and diplotene spermatocyte population (Figure 5F). This finding suggests that meiotic progression of *Cep215* KO male germ cells is predominantly arrested around the zygotene stage.

### 3.6 | Intact centrosomes in *Cep215* KO testis cells

We conducted immunohistochemistry to investigate subcellular distribution of Cep215 in the male germ cells. The centrioles of premeiotic and postmeiotic germ cells were labeled with the centrin-2 antibody (Figure 6A). Additionally, pericentriolar material (PCM) proteins were evident in the centrosomes of male germ cells, except for round spermatids immediately after meiosis (Figure 6A). Cep215 signals were observed at the centrosomes of all male germ cells, co-localizing with the centrin-2, pericentrin, and  $\gamma$ -tubulin signals (Figure 6A). In *Cep215* KO testes, Cep215 was absent, but other centrosome proteins were still detectable at male germ cell centrosomes (Figure 6A). Notably, *Cep215* KO male germ cells retained normal numbers of centrioles surrounded by PCM proteins (Figure 6A), suggesting that centrosomes in male germ cells remain largely intact even in the absence of Cep215.

To further investigate centrosomes during meiosis, we isolated male germ cells from P17 mice and conducted coimmunostaining analyses. It is established that centriole duplication and separation occur at zygotene and diakinesis of meiotic prophase I, respectively.<sup>40–42</sup> Despite the absence of Cep215 in the centrosomes, the expected numbers of centrioles were detected in spermatogonia and spermatocytes (Figure 6B–D). Precocious centriole separation was not observed in *Cep215*-deleted male germ cells, indicating that centriole duplication and separation proceed normally in *Cep215* KO male germ cells (Figure 6B). We assessed the centrosome intensities of selected PCM proteins in isolated spermatocytes. While the levels of  $\gamma$ -tubulin at the centrosomes were reduced in *Cep215* KO spermatocytes, those of pericentrin remained unchanged (Figure 6E,F). These findings align with observations in *Cep215*-deleted culture cells, suggesting that while centrosome composition may be affected in the absence of Cep215, cell division still occurs.<sup>43</sup>

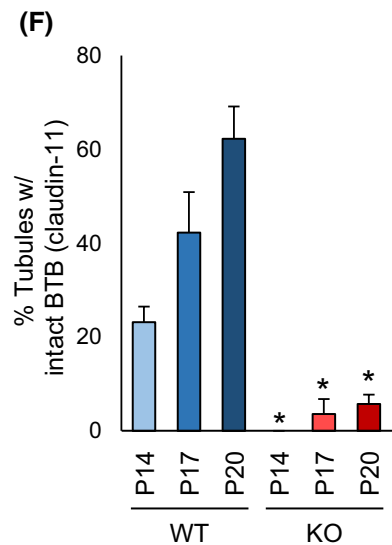
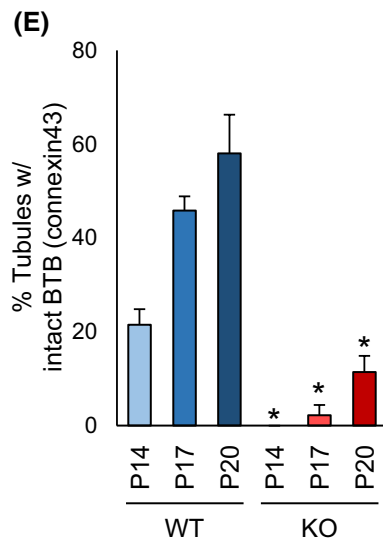
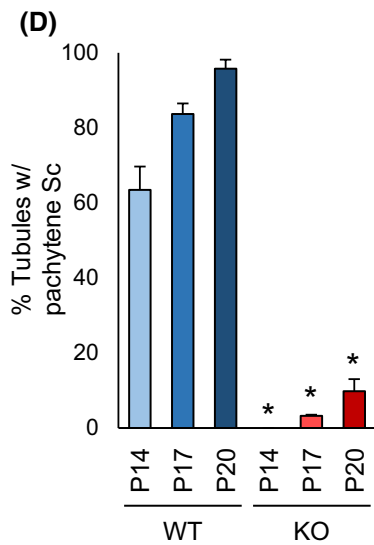
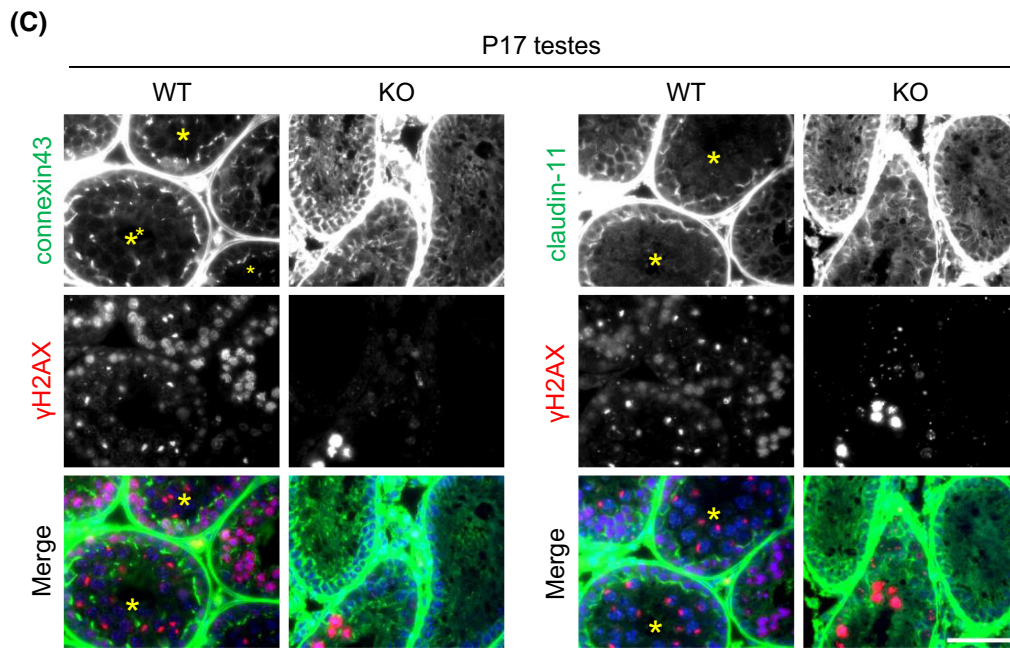
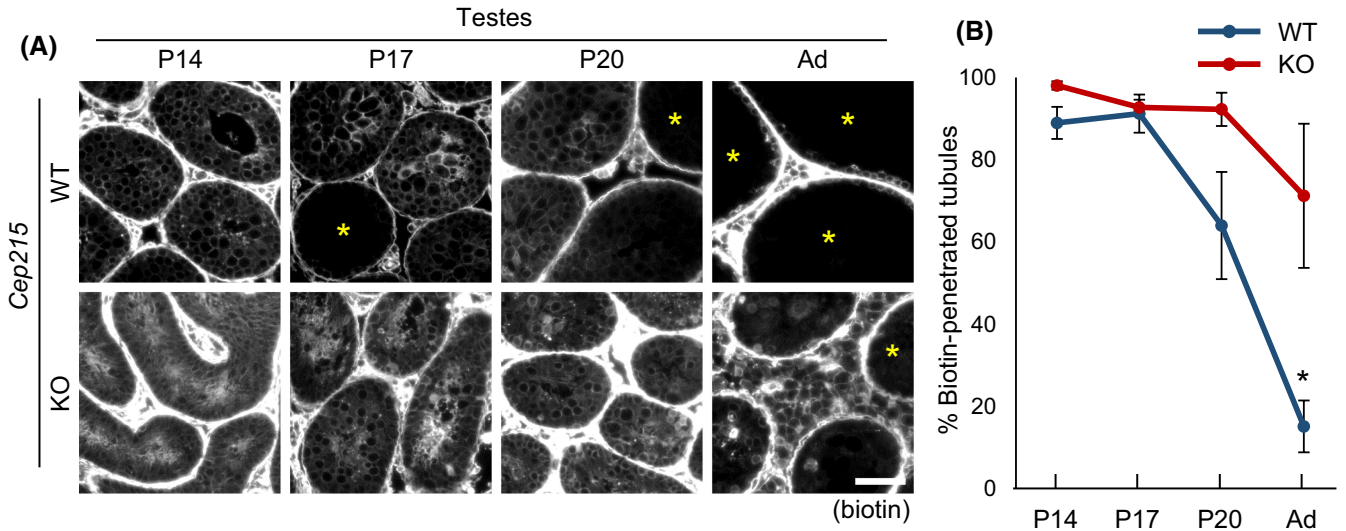


**FIGURE 8** Failure of the blood–testis barrier (BTB) in the *Cep215* KO testes. (A) The biotin-penetration assays with the *Cep215* KO mice at indicated ages. (B) The number of biotin-penetrated seminiferous tubules was counted. More than 100 tubules per experimental group were analyzed. (C) Immunohistochemistry of the testes of *Cep215* KO mice at P17 with connexin-43 (green), claudin-11 (green), and  $\gamma$ H2AX (red) antibodies. Nuclei were stained with DAPI (blue). (D) The number of tubules containing pachytene spermatocytes was counted. (E, F) The number of tubules with intact BTB structure was counted. The intactness of BTB was determined with the immunostaining staining patterns of connexin-43 (E) and claudin-11 (F). At least 200 tubules per experimental group were analyzed ( $n = 3$ ). (A, C) Stars represent seminiferous tubules with intact BTB. Scale bars: 50  $\mu$ m. (B, D, E, F) Values are means and SEM. The statistical significance was determined by two-way ANOVA. \* $p < .05$ , compared to the wild type.

We explored the role of *Cep215* in Sertoli cells, which are identified by vimentin antibodies.<sup>23</sup> Centrioles in Sertoli cells were visualized using centrin-2 antibody (Figure 7A). The results revealed that PCM of the *Cep215* KO Sertoli cells was coimmunostained with pericentrin and  $\gamma$ -tubulin antibodies but not with *Cep215* antibody (Figure 7A). For a more detailed examination, we isolated Sertoli cells and depleted *Cep215* using siRNAs, and coimmunostained them with centrosome-specific antibodies (Figure 7B). Our results demonstrated that depletion of *Cep215* did not significantly affect centrosome intensities of centrin-2 and pericentrin, whereas those of  $\gamma$ -tubulin were reduced (Figure 7C–F). These findings suggest that *Cep215* recruits  $\gamma$ -tubulin at the centrosome of Sertoli cells and may contribute to the regulation of microtubule organization in Sertoli cells, similar to its function in other cellular contexts.

### 3.7 | Defects in the testis architecture of *Cep215* KO mice

Previous data indicating that *Cep215* KO male germ cells possess normal numbers of centrosomes with mostly intact PCM, yet undergo apoptosis prior to meiosis, lead us to speculate that subtle changes in the architecture of *Cep215* KO testes may be attributed to apoptosis in premeiotic germ cells. Sertoli cells play a pivotal role in establishing tight junctions, forming BTB, which segregates seminiferous tubules into basal and adluminal compartments.<sup>44</sup> The BTB is crucial for completion of meiosis during postnatal development of male germ cells. Upon differentiation of spermatogonia to preleptotene spermatocytes, they are transferred from the basal to the adluminal compartment for further progression to meiosis.<sup>45</sup> If the BTB is not properly installed, the development of male germ cells is impeded, and they are eventually eliminated from the tubules via apoptosis.<sup>45–47</sup>

To investigate the hypothesis that the BTB might be compromised in *Cep215* KO testes, we conducted biotin-penetration assays. In wild-type mice, fluorescent-tagged biotin signals were detected in the luminal side of seminiferous tubules until P17, after which they gradually diminished, reaching minimal levels in adults (Figure 8A,B).

These observations are consistent with the establishment of the BTB at P18, prior to meiosis.<sup>46</sup> However, in *Cep215* KO mice, biotin signals were consistently detected in the lumen of both immature and adult testes, indicating a leaky BTB in these mice.

To evaluate whether *Cep215* deletion affects BTB formation, we conducted immunohistochemistry on immature testes using antibodies against BTB component proteins, such as connexin-43 and claudin-11, along with the  $\gamma$ H2AX antibody for detection of premeiotic germ cells (Figure 8C).<sup>48</sup> While most seminiferous tubules from wild-type mice contained pachytene spermatocytes at P20, those from *Cep215* KO mice exhibited sparse presence of these cells (Figure 8D). In wild-type testes, both connexin-43 and claudin-11 formed a ring-like structure, dividing seminiferous tubules into basal and adluminal compartments (Figure 8C,E,F). However, in *Cep215* KO testes, these proteins hardly formed a ring-like structure but remained periphery of the Sertoli cells even at P20 (Figure 8C,E,F). These findings collectively support the notion that the BTB is not properly established in *Cep215* KO testes.

## 4 | DISCUSSION

In this study, we generated KO mice in which most regions of the *Cep215* locus was removed. These *Cep215* KO mice exhibit partial embryonic lethality, and thus only half of the *Cep215* homozygous KO mice are born and survive. Notably, the *Cep215* KO mice manifest typical phenotypes previously reported in the *Cep215*<sup>an/an</sup> mutant mice, including microcephaly, eye defects, and male sterility.<sup>16–19</sup> These observations confirm that while *Cep215* may be dispensable for postnatal survival, but the deficiency significantly disrupts the normal development of specific organs, such as brain, eye, and testis.

*Cep215* is predominantly expressed in the testis, likely due to the high proliferation activity of male germ cells. Signals of *Cep215* were consistently detected at the centrosomes in male germ cells throughout all developmental stages, except at haploid cells immediately after meiosis. Considering the role of *Cep215* as a PCM protein involved in microtubule organization

at spindle poles, one might anticipate that its deletion would disrupt meiosis. However, we are hesitant to interpret that spindle defects are attributed to meiotic arrest of the *Cep215* germ cells per se. First, most *Cep215* KO male germ cells halt their development at zygotene and pachytene stages, where meiotic spindles are yet to assemble. Secondly, despite the absence of *Cep215*, centrosomes in the *Cep215* KO male germ cells remain largely intact, with comparable amounts of pericentrin to wild-type cells. While levels of  $\gamma$ -tubulin at the centrosomes appear reduced, this reduction is unlikely to completely block division of *Cep215* KO spermatocytes.<sup>6,43</sup> Thirdly, the meiosis surveillance pathway, induced by a prolonged mitosis and leading to p53-dependent apoptosis, may not be activated in *Cep215* KO testes.<sup>49,50</sup> Finally, *Cep215* KO females have functional oocytes and are fertile, indicating that meiosis proceeds normally in oocytes (data not shown). Taken together, these findings strongly suggest that meiotic arrest of *Cep215* KO male germ cells may not directly result from defects in spindle assembly. Instead, it is plausible that combinatorial defects in the testis contribute to the meiotic prophase arrest of *Cep215* KO male germ cells.

We observed that the failure of BTB formation leads to meiotic arrest at the zygotene stage in immature testes.<sup>46</sup> Indeed, we confirmed that the BTB is not properly established in the *Cep215* KO testes. These observations suggest that BTB failure contributes to male germ cell defects in the *Cep215* KO mice at least in part (Figure 9). Our interpretation is supported by a previous report in which BTB is disturbed in the absence of *Akap9*, a centrosome protein.<sup>52</sup> Microtubule networks are disturbed in Sertoli cells of the *Akap9* KO mice, resulting in the arrest of germ cell development at premeiotic phase.<sup>51–53</sup>

It remains to be investigated why the BTB is not properly formed in the *Cep215* KO testes. It is plausible that in *Cep215* KO Sertoli cells, the cytoskeletal structure is disturbed. *Cep215* not only organizes microtubules at the centrosomes but also at other subcellular organelles, such as the nuclear membrane, endoplasmic reticulum, and Golgi apparatus, regulating cell morphology and motility.<sup>54,55</sup> Microtubules in Sertoli cells play a crucial role in cell morphology and movement.<sup>51</sup> Disruption of Sertoli cell polarity may hinder proper development of male germ cells, leading to arrest at a premeiotic stage.<sup>23,56</sup> The pattern of microtubule regrowth in Sertoli cells indicates that their primary nucleation site is the apical sites of Sertoli cells.<sup>57</sup> Moreover, when  $\gamma$ -tubulin is overexpressed in Sertoli cells, exogenous  $\gamma$ -tubulin localizes at the apical sites, causing redistribution of microtubules and disrupting the histology of testes.<sup>58</sup> Based on these observations, the role of *Cep215* in Sertoli cells may involve regulating microtubule networks by promoting the nucleation of noncentrosomal

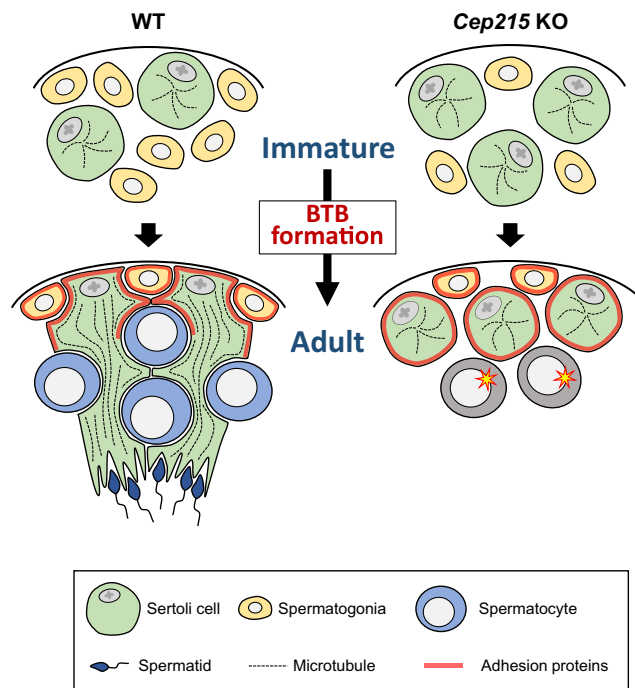


**FIGURE 9** Model in immature testes, seminiferous tubules comprise spermatogonial stem cells and Sertoli cells. During puberty in mice, Sertoli cells undergo polarization and establish interactions with neighboring Sertoli cells, culminating in the formation of BTB. This process involves the rearrangement of microtubules parallel to the polarity of Sertoli cell, facilitating proper cell–cell interactions and barrier formation.<sup>51</sup> In *Cep215* KO testes, the proliferation activity of the spermatogonial stem cells decreases and Sertoli cells fail to polarize, possibly due to microtubule misorientation. Consequently, BTB is not formed and spermatogenesis is blocked prior to meiosis in *Cep215* KO mice.

microtubules at apical processes. Consequently, *Cep215* deletion may disturb the cellular structures of Sertoli cells, leading to loss of cell polarity and cell–cell interactions required for BTB formation (Figure 9).

Another possibility may be that delay in cell division of *Cep215* KO male germ cells negatively modulates BTB formation.<sup>59</sup> It is known that early spermatocytes take a role in BTB assembly by expressing claudin-3 for a transient adhesion between Sertoli cells and germ cells.<sup>25</sup> If the number of male germ cells is not sufficient enough, BTB may not be formed at a right time for male germ cell development. We showed that the number of male germ cells in *Cep215* KO testes is significantly smaller than that in the wild-type testes, as a result of extended mitosis in the absence of *Cep215*.<sup>60</sup> Reduction in the male germ cell numbers in *Cep215* KO testes might be attributed to failure in initial interaction between Sertoli cells and male germ cells and eventually failure in BTB formation (Figure 9). In fact, abnormal assembly of mitotic spindles has been pointed out in interpreting *Cep215* KO phenotypes of microcephaly and macrocytic anemia.<sup>16,21</sup> Last, it is known



that BTB formation is regulated by androgen.<sup>45</sup> We cannot rule out the possibility that hormonal factors contribute to the failure of BTB formation, even if no significant difference in Leydig cell numbers was observed between the wild-type and mutant testes at immature stages.

A common consequence of centrosome loss may involve the activation of the mitotic surveillance pathway, leading to elevated p53 levels after prolonged mitosis. Indeed, co-deletion of *Trp53* has been shown to alleviate the severity of phenotypes observed in deletions of the centrosome genes, such as *Sas4/Cpap* and *Sas6*.<sup>39,61,62</sup> However, in case of *Cep215* KO mice, the phenotypic rescue was not observed upon co-deletion of *Trp53*. Notably, defects in erythrocyte differentiation in *Cep215* KO mice were also unaffected by co-deletion of *Trp53*.<sup>21</sup> These results strongly suggest that the meiotic surveillance pathway may not be activated in *Cep215* KO mice. While mitotic and meiotic progression may be delayed in *Cep215* KO cells, such delay may not reach the threshold for activation of the mitotic surveillance pathway.<sup>38</sup> Nonetheless, even a slight delay in cell division could result in a reduction in cell number, ultimately leading to a meiotic arrest in conjunction with other defects, such as malfunctioning Sertoli cells.<sup>60</sup>

In this work, we propose that *Cep215* deletion results in the arrest of male germ cells at meiotic prophase, potentially due to a combination of delayed cell division and altered Sertoli cell structure. Moreover, we speculate that microcephaly observed in *Cep215* KO mice may arise from a combination of factors, including a slight delay in the proliferation of neural stem cells, misorientation of the division plane, and impaired cell migration.

#### AUTHOR CONTRIBUTIONS

Kunsoo Rhee and Young Hoon Sung designed research; Donghee Kang, Byungho Shin, Gyeong-Nam Kim, and Ji Hwa Hea performed experiments; Gyeong-Nam Kim and Ji Hwa Hea generated and maintained KO mice; Donghee Kang performed data analysis and prepared all figures; Donghee Kang, Kunsoo Rhee, and Young Hoon Sung wrote the paper. All authors read and approved the final manuscript.

#### ACKNOWLEDGMENTS

This work was supported by the National Research Foundation of Korea (NRF; Grant Numbers RS-2024-00344272 to K.R.; 2014M3A9D5A01075128 to Y.H.S.) funded by the Ministry of Science, ICT, and Future Planning (Grant Number HI21C169202 to Y.H.S.) of the Korea Health Technology R&D Project through the Korea Health Industry Development Institute (KHIDI) funded by the Ministry of Health & Welfare, Republic of Korea and by a grant (2021IP0050 to Y.H.S.) from the Asan Institute for Life Sciences, Asan Medical Center, Seoul,

Republic of Korea. We thank the core facilities of the Mammalian Genetics Core and the GEAR Core at Asan Institute for Life Sciences for the shared equipment and expertise support.

#### DISCLOSURES

The authors declare no conflicts of interest.

#### DATA AVAILABILITY STATEMENT

The data that support the findings of this study are available upon request from the corresponding authors.

#### ORCID

Donghee Kang  <https://orcid.org/0009-0003-2326-3700>

Byungho Shin  <https://orcid.org/0000-0002-6287-5991>

Ji Hwa Hea  <https://orcid.org/0009-0003-0426-2593>

Young Hoon Sung  <https://orcid.org/0000-0002-1508-9883>

Kunsoo Rhee  <https://orcid.org/0000-0002-5051-876X>

#### REFERENCES

- Megraw TL, Sharkey JT, Nowakowski RS. Cdk5rap2 exposes the centrosomal root of microcephaly syndromes. *Trends Cell Biol.* 2011;21:470-480.
- Zhang J, Megraw TL. Proper recruitment of gamma-tubulin and D-TACC/Msps to embryonic *Drosophila* centrosomes requires Centrosomin Motif 1. *Mol Biol Cell.* 2007;18:4037-4049.
- Fong KW, Choi YK, Rattner JB, Qi RZ. CDK5RAP2 is a pericentriolar protein that functions in centrosomal attachment of the gamma-tubulin ring complex. *Mol Biol Cell.* 2008;19:115-125.
- Choi YK, Liu P, Sze SK, Dai C, Qi RZ. CDK5RAP2 stimulates microtubule nucleation by the gamma-tubulin ring complex. *J Cell Biol.* 2010;191:1089-1095.
- Lee S, Rhee K. CEP215 is involved in the dynein-dependent accumulation of pericentriolar matrix proteins for spindle pole formation. *Cell Cycle.* 2010;9:775-784.
- Barr AR, Kilmartin JV, Gergely F. CDK5RAP2 functions in centrosome to spindle pole attachment and DNA damage response. *J Cell Biol.* 2010;189:23-39.
- Kim S, Rhee K. Importance of the CEP215-pericentriolar interaction for centrosome maturation during mitosis. *PLoS One.* 2014;9:e87016.
- Wang Z, Wu T, Shi L, et al. Conserved motif of CDK5RAP2 mediates its localization to centrosomes and the Golgi complex. *J Biol Chem.* 2010;285:22658-22665.
- Bond J, Roberts E, Springell K, et al. A centrosomal mechanism involving CDK5RAP2 and CENPJ controls brain size. *Nat Genet.* 2005;37:353-355.
- Marthiens V, Basto R. Centrosomes: the good and the bad for brain development. *Biol Cell.* 2020;112:153-172.
- Hassan MJ, Khurshid M, Azeem Z, et al. Previously described sequence variant in *CDK5RAP2* gene in a Pakistani family with autosomal recessive primary microcephaly. *BMC Med Genet.* 2007;8:58.
- Alfares A, Alhufayti I, Alsubaie L, et al. A new association between CDK5RAP2 microcephaly and congenital cataracts. *Ann Hum Genet.* 2018;82:165-170.

13. Makhdoom EUH, Anwar H, Baig SM, Hussain G. Whole exome sequencing identifies a novel mutation in *ASPM* and ultra-rare mutation in *CDK5RAP2* causing primary microcephaly in consanguineous Pakistani families. *Pak J Med Sci.* 2022;38:84-89.
14. Hertwig P. Neue Mutationen und Koppelungsgruppen bei der Hausmaus. *Z Indukt Abstamm Vererbungsl.* 1942;80:220-246.
15. Barker JE, Deveau SA, Compton ST, Fancher K, Eppig JT. High incidence, early onset of histiocytic sarcomas in mice with Hertwig's anemia. *Exp Hematol.* 2005;33:1118-1129.
16. Lizarraga SB, Margossian SP, Harris MH, et al. Cdk5rap2 regulates centrosome function and chromosome segregation in neuronal progenitors. *Development.* 2010;137:1907-1917.
17. Zaqout S, Bessa P, Kramer N, Stoltenburg-Didinger G, Kaindl AM. CDK5RAP2 is required to maintain the germ cell pool during embryonic development. *Stem Cell Reports.* 2017;8:198-204.
18. Zaqout S, Blaesius K, Wu YJ, et al. Altered inhibition and excitation in neocortical circuits in congenital microcephaly. *Neurobiol Dis.* 2019;129:130-143.
19. Zaqout S, Ravindran E, Stoltenburg-Didinger G, Kaindl AM. Congenital microcephaly-linked CDK5RAP2 affects eye development. *Ann Hum Genet.* 2020;84:87-91.
20. Barrera JA, Kao LR, Hammer RE, Seemann J, Fuchs JL, Megraw TL. CDK5RAP2 regulates centriole engagement and cohesion in mice. *Dev Cell.* 2010;18:913-926.
21. Tatrai P, Gergely F. Centrosome function is critical during terminal erythroid differentiation. *EMBO J.* 2022;41:e108739.
22. Mouse genome informatics. Accessed June 14, 2024. <https://www.informatics.jax.org/>
23. Heinrich A, Potter SJ, Guo L, Ratner N, DeFalco T. Distinct roles for *rac1* in sertoli cell function during testicular development and spermatogenesis. *Cell Rep.* 2020;31:107513.
24. Griswold MD. 50 years of spermatogenesis: Sertoli cells and their interactions with germ cells. *Biol Reprod.* 2018;99:87-100.
25. Smith BE, Braun RE. Germ cell migration across Sertoli cell tight junctions. *Science.* 2012;338:798-802.
26. Shen B, Zhang W, Zhang J, et al. Efficient genome modification by CRISPR-Cas9 nickase with minimal off-target effects. *Nat Methods.* 2014;11:399-402.
27. Oh SH, Lee HJ, Ahn MK, et al. Multiplex gene targeting in the mouse embryo using a Cas9-Cpf1 hybrid guide RNA. *Biochem Biophys Res Commun.* 2021;539:48-55.
28. Kim Y, Cheong SA, Lee JG, et al. Generation of knockout mice by Cpf1-mediated gene targeting. *Nat Biotechnol.* 2016;34:808-810.
29. Kaneko T, Mashimo T. Simple genome editing of rodent intact embryos by electroporation. *PLoS One.* 2015;10:e0142755.
30. Kim K, Rhee K. The pericentriolar satellite protein CEP90 is crucial for integrity of the mitotic spindle pole. *J Cell Sci.* 2011;124:338-347.
31. Gopinathan L, Szmyd R, Low D, et al. Emi2 is essential for mouse spermatogenesis. *Cell Rep.* 2017;20:697-708.
32. Ahmadi H, Boroujeni ME, Sadeghi Y, et al. Sertoli cells avert neuroinflammation-induced cell death and improve motor function and striatal atrophy in rat model of huntington disease. *J Mol Neurosci.* 2018;65:17-27.
33. Gimpel P, Lee YL, Sobota RM, et al. Nesprin-1alpha-dependent microtubule nucleation from the nuclear envelope via akap450 is necessary for nuclear positioning in muscle cells. *Curr Biol.* 2017;27:2999-3009.
34. Kraemer N, Issa-Jahns L, Neubert G, et al. Novel alternative splice variants of mouse *Cdk5rap2*. *PLoS One.* 2015;10:e0136684.
35. Nebel BR, Amarose AP, Hacket EM. Calendar of gametogenic development in the prepuberal male mouse. *Science.* 1961;134:832-833.
36. McLean DJ, Friel PJ, Johnston DS, Griswold MD. Characterization of spermatogonial stem cell maturation and differentiation in neonatal mice. *Biol Reprod.* 2003;69:2085-2091.
37. Curley M, Gonzalez ZN, Milne L, et al. Human adipose-derived pericytes display steroidogenic lineage potential in vitro and influence Leydig cell regeneration in vivo in rats. *Sci Rep.* 2019;9:15037.
38. Meyer-Gerards CP, Bazzi H. Developmental and tissue-specific roles of mammalian centrosomes. *FEBS J.* 2024. <https://doi.org/10.1111/febs.17212>
39. Bazzi H, Anderson KV. Acentriolar mitosis activates a p53-dependent apoptosis pathway in the mouse embryo. *Proc Natl Acad Sci U S A.* 2014;111:E1491-E1500.
40. Lee J, Kim S, Jeong Y, Rhee K. Centrobin/Nip2 expression in vivo suggests its involvement in cell proliferation. *Mol Cells.* 2009;28:31-36.
41. Alfaro E, Lopez-Jimenez P, Gonzalez-Martinez J, Malumbres M, Suja JA, Gomez R. PLK1 regulates centrosome migration and spindle dynamics in male mouse meiosis. *EMBO Rep.* 2021;22:e51030.
42. Wellard SR, Zhang Y, Shults C, et al. Overlapping roles for PLK1 and Aurora a during meiotic centrosome biogenesis in mouse spermatocytes. *EMBO Rep.* 2021;22:e51023.
43. Jung GI, Rhee K. Triple deletion of TP53, PCNT, and CEP215 promotes centriole amplification in the M phase. *Cell Cycle.* 2021;20:1500-1517.
44. O'Donnell L, Smith LB, Rebourcet D. Sertoli cells as key drivers of testis function. *Semin Cell Dev Biol.* 2022;121:2-9.
45. Mruk DD, Cheng CY. The mammalian blood-testis barrier: its biology and regulation. *Endocr Rev.* 2015;36:564-591.
46. Morales A, Mohamed F, Cavicchia JC. Apoptosis and blood-testis barrier during the first spermatogenic wave in the pubertal rat. *Anat Rec.* 2007;290:206-214.
47. Luaces JP, Toro-Urrego N, Otero-Losada M, Capani F. What do we know about blood-testis barrier? Current understanding of its structure and physiology. *Front Cell Dev Biol.* 2023;11:1114769.
48. Hollenbach J, Jung K, Noelke J, et al. Loss of connexin43 in murine Sertoli cells and its effect on blood-testis barrier formation and dynamics. *PLoS One.* 2018;13:e0198100.
49. Phan TP, Holland AJ. Time is of the essence: the molecular mechanisms of primary microcephaly. *Genes Dev.* 2021;35:1551-1578.
50. Phan TP, Maryniak AL, Boatwright CA, et al. Centrosome defects cause microcephaly by activating the 53BP1-USP28-TP53 mitotic surveillance pathway. *EMBO J.* 2021;40:e106118.
51. Wu S, Li L, Wu X, Wong CKC, Sun F, Cheng CY. AKAP9 supports spermatogenesis through its effects on microtubule and actin cytoskeletons in the rat testis. *FASEB J.* 2021;35:e21925.
52. Venkatesh D, Mruk D, Herter JM, et al. AKAP9, a regulator of microtubule dynamics, contributes to blood-testis barrier function. *Am J Pathol.* 2016;186:270-284.
53. Schimenti KJ, Feuer SK, Griffin LB, et al. AKAP9 is essential for spermatogenesis and Sertoli cell maturation in mice. *Genetics.* 2013;194:447-457.

54. Sanchez AD, Feldman JL. Microtubule-organizing centers: from the centrosome to non-centrosomal sites. *Curr Opin Cell Biol.* 2017;44:93-101.
55. Ide K, Muko M, Hayashi K. The Golgi apparatus is the main microtubule-organizing center in differentiating skeletal muscle cells. *Histochem Cell Biol.* 2021;156:273-281.
56. Heinrich A, Bhandary B, Potter SJ, Ratner N, DeFalco T. Cdc42 activity in Sertoli cells is essential for maintenance of spermatogenesis. *Cell Rep.* 2021;37:109885.
57. Vogl AW, Weis M, Pfeiffer DC. The perinuclear centriole-containing centrosome is not the major microtubule organizing center in Sertoli cells. *Eur J Cell Biol.* 1995;66:165-179.
58. Fleming SL, Shank PR, Boekelheide K. gamma-Tubulin over-expression in Sertoli cells in vivo: I. Localization to sites of spermatid head attachment and alterations in Sertoli cell microtubule distribution. *Biol Reprod.* 2003;69:310-321.
59. Li XY, Zhang Y, Wang XX, et al. Regulation of blood-testis barrier assembly in vivo by germ cells. *FASEB J.* 2018;32:1653-1664.
60. Meitinger F, Belal H, Davis RL, et al. Control of cell proliferation by memories of mitosis. *Science.* 2024;383:1441-1448.
61. Xiao C, Grzonka M, Meyer-Gerards C, Mack M, Figge R, Bazzi H. Gradual centriole maturation associates with the mitotic surveillance pathway in mouse development. *EMBO Rep.* 2021;22:e51127.
62. Grzonka M, Bazzi H. Mouse SAS-6 is required for centriole formation in embryos and integrity in embryonic stem cells. *elife.* 2024;13:e94694.

**How to cite this article:** Kang D, Shin B, Kim G-N, Hea JH, Sung YH, Rhee K. Roles of Cep215/Cdk5rap2 in establishing testicular architecture for mouse male germ cell development. *The FASEB Journal.* 2024;38:e70188. doi:[10.1096/fj.202401541R](https://doi.org/10.1096/fj.202401541R)